PHYSICAL REVIEW B VOLUME 56, NUMBER 3 15 JULY 1997-I

Electron mobility in $Al_xGa_{1-x}N$/GaN heterostructures

L. Hsu
Department of Physics, University of California, Berkeley, California 94720
and Materials Science Division, Lawrence Berkeley National Laboratory, Berkeley, California 94720

W. Walukiewicz
Materials Science Division, Lawrence Berkeley National Laboratory, Berkeley, California 94720
(Received 27 January 1997)

Theoretical electron mobility limits of a two-dimensional electron gas (2DEG) confined near the interface of a $Al_xGa_{1-x}N$/GaN heterostructure are computed. The electronic structure of the 2DEG is calculated self-consistently to obtain the best analytic solution for the wave functions, and the results are used to compute the mobilities. All standard scattering mechanisms, including scattering by acoustic and optical phonons, remote and background impurities, and alloy disorder have been included in our calculations. Depending on the exact composition of the heterostructure, the low-temperature mobility may be limited by either Coulomb or alloy disorder scattering. Strategies for optimizing the mobility for various remote doping concentrations and spacer widths are discussed. Intrinsic mobilities in excess of 10^6 cm^2/V s are predicted for optimized heterostructures at low temperatures. [S0163-1829(97)08728-6]

I. INTRODUCTION

The interaction of electrons with charged impurity centers is the dominant mechanism responsible for the scattering of free electrons at low temperatures in doped, high-quality semiconductors. In order to reduce this interaction and increase the low temperature mobility, it was proposed by Esaki and Tsu in 1969 (Ref. 1) that one could separate the carriers from the parent donors by growing a modulation-doped heterostructure (MDH). However, it was not until the late seventies that the molecular-beam-epitaxy (MBE) technique was sufficiently developed to grow such structures.[2] Subsequent studies involving the $Al_xGa_{1-x}As$/GaAs system showed that electron mobilities could be increased up to three orders of magnitude in MDH's as compared to bulk GaAs.[3–5] This discovery was the foundation for the creation and development of high-speed GaAs semiconductor devices. Concurrent with the experimental development of these $Al_xGa_{1-x}As$/GaAs heterostructures, there was a burst of theoretical work aimed at modeling the electron mobilities in these structures.[6–9] By now, the electron transport behavior in these materials is well understood.

In the past five years, GaN has been the focus of intense research. Due to its large band gap, tunable between 1.9 and 6.2 eV upon alloying with In or Al and its high thermal conductivity and stability, GaN is ideally suited for making light-emitting diodes, lasers, and detectors operating in the visible to ultraviolet range as well as high-power transistors with operating frequencies in the microwave regime.[10–12] Based on the experience with GaAs, it was natural to grow $Al_xGa_{1-x}N$/GaN MDH's to try to maximize the electron mobilities in GaN, and thus the operating characteristics of GaN-based devices as well. Several attempts have been made with a fair degree of success.[13–15] Some estimates of theoretical mobility limits in these structures have been made using a three-dimensional approximation[16] which, although accurate at room temperature, is not suitable for low temperatures, and cannot properly describe the scattering from remote impurities, which is the most important characteristic of modulation-doped structures. However, no rigorous calculations on the same level as those made for $Al_xGa_{1-x}As$/GaAs MDHs have been performed, to our knowledge.

In this paper, we report on the results of such computations. All major scattering mechanisms, including acoustic and optical phonons, ionized impurities, and alloy disorder, have been taken into account. In Sec. II the electronic structure of the 2DEG in the $Al_xGa_{1-x}N$/GaN MDH is described. Section III discusses the mobility calculations in detail. The results of the calculations as well as their relation to experimentally obtained mobilities are the focus of Sec. IV. Finally, we summarize our results in Sec. V.

II. ELECTRONIC STRUCTURE OF THE 2DEG

The conduction-band structure of a $Al_xGa_{1-x}N$/GaN heterostructure near the interface is shown in Fig. 1. In the ideal case, the GaN (at $z\geqslant 0$) is nominally undoped while the $Al_xGa_{1-x}N$/GaN ($z\leqslant 0$) is selectively doped and consists of a nominally undoped region ($0\geqslant z\geqslant -d$) known as the ''spacer'' and an intentionally doped region ($z\leqslant -d$). As GaN has a higher affinity for electrons than $Al_xGa_{1-x}N$, electrons from the donors in the $Al_xGa_{1-x}N$ are transferred to the GaN. The positively charged donors in the $Al_xGa_{1-x}N$ produce an electric field which creates a potential well in the GaN, confining the electrons to a narrow strip at the interface, and leading to a quantization of the energy-band structure into subbands. At equilibrium, the transfer of electrons from the $Al_xGa_{1-x}N$ to the GaN is determined by the equation

$$V_0-\frac{4\pi e^2}{\varepsilon_S}(N_S+N_{\rm depl})d-\frac{4\pi e^2}{2\varepsilon_S}\frac{(N_S+N_{\rm depl})^2}{N_I}=E_F, \tag{1}$$

0163-1829/97/56(3)/1520(9)/$10.00 © 1997 The American Physical Society

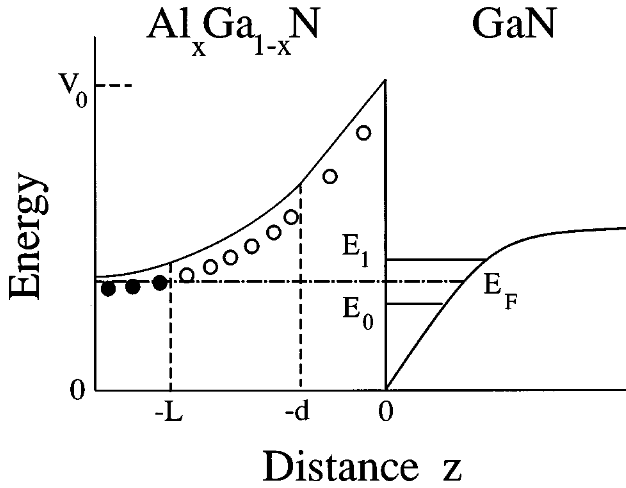

FIG. 1. Schematic diagram of the energy subbands in a single-quantum-well modulation-doped heterostructure, showing the lowest two energy bands, Fermi energy, and both neutral (closed circles) and ionized (open circles) impurities in the $Al_xGa_{1-x}N$ layer.

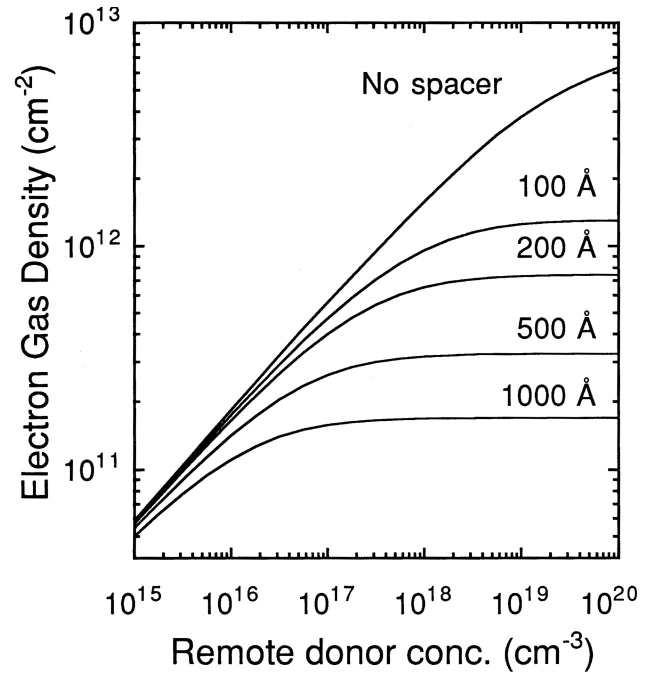

FIG. 2. Graph of Eq. (1), showing two-dimensional electron gas density in the GaN as a function of $Al_{0.15}Ga_{0.85}N$ doping concentration (N_1) for various spacer widths (d).

where V_0, E_F, and spacer width d are as shown in Fig. 1. N_S is the areal (two-dimensional) electron concentration in the GaN, $N_{\rm depl}$ is the areal concentration of residual charged impurities in the GaN, N_I is the bulk concentration of so-called "remote" donors in the $Al_xGa_{1-x}N$, and ε_S is the static dielectric constant of GaN. Assuming that only one subband is occupied, the Fermi energy E_F is given by

$$E_F = E_0 + \frac{\pi\hbar^2}{m^*} N_S, \tag{2}$$

where $m^*/\pi\hbar^2$ is the two-dimensional density of states in GaN, and E_0 is the energy of the lowest subband. In most cases, $N_{\rm depl}$, the product of the bulk residual charged impurity concentration and the effective width of the electron gas, can be made at least two orders of magnitude smaller than N_S, and thus can be neglected in this equation. In Fig. 2, the two-dimensional electron-gas density is shown as a function of the $Al_xGa_{1-x}N$ doping level for a $Al_{0.15}Ga_{0.85}N/GaN$ structure with a variety of spacer widths.

In order to determine the GaN conduction-band structure and quantized energy levels of the 2DEG, Poisson's equation

$$\nabla^2\phi = -\frac{4\pi\rho}{\varepsilon} = -\frac{4\pi}{\varepsilon}|\psi|^2, \tag{3}$$

and Schrödinger's equation with GaN effective mass m^*,

$$-\frac{\hbar^2}{2m^*}\nabla^2\psi + V(z)\psi = E\psi, \tag{4}$$

must be solved self-consistently for the electronic wave function.[17] In our calculations, the potential-energy term consists of the electrostatic potential energy as well as the exchange-correlation energy of the electrons. The form of the exchange correlation energy was taken from a paper by Hautmann and Sander,[18] who used an expression derived by Gunnarsson and Lundqvist.[19]

In order to solve the two coupled equations, we started with a trial wavefunction with one free parameter and, using Poisson's equation, calculated an expression for the potential energy of the electrons which contained the parameter. A simple variational calculation to minimize the total energy of the electrons was performed to determine the value of the parameter. Using this value, the resulting expression for the potential energy was inserted into the Schrödinger equation (4) to determine the electronic energy levels and another wave function. This wave function could then be compared to the old one. Naturally, an exact solution to both equations can only be found numerically, but our intention was to find the closest possible analytic approximation to the true answer.

Previous calculations of 2DEG in Si and in the $Al_xGa_{1-x}As/GaAs$ system have shown that

$$\psi_0 = \phi_{x,y}\chi(z) = \phi_{x,y}\left(\frac{b^3}{2}\right)^{1/2} z\,\exp(-bz/2), \tag{5}$$

where $\phi_{x,y}$ is a two dimensional plane-wave wave function and b is a variational parameter, is a good approximation to the electronic wave function of the lowest subband. Using this as our starting ground-state electron wave function, we tried a number of different analytic forms, finding that

$$\chi(z) = \frac{b^2}{\sqrt{6}} z^{3/2}\exp(-bz/2). \tag{6}$$

minimized the energy of the electrons. The parameter b, of course, depends on the electron-gas density and is a measure of the width of the 2DEG. As a function of the electron density, b varies roughly as $N_s^{0.315}$.

In Fig. 3, we show the energy levels of the lowest three subbands as a function of the electron-gas density. As can be seen, only the lowest subband is occupied for electron concentrations below 4.5×10^{12} cm^{-2}. At greater concentra-

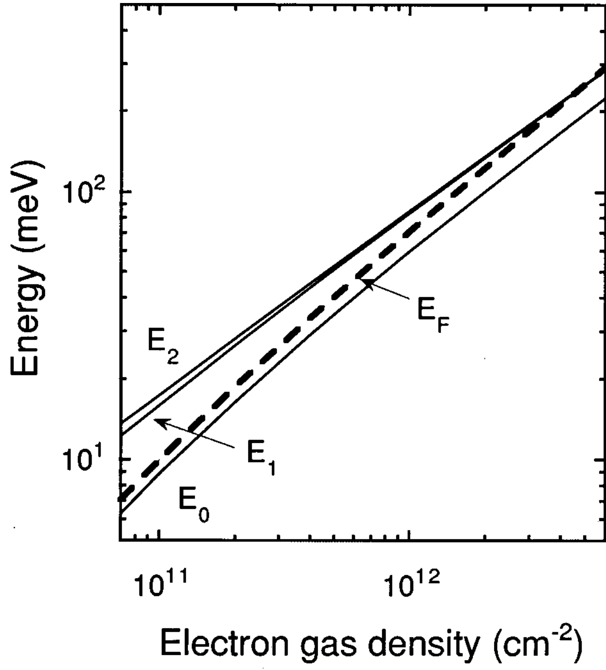

FIG. 3. The lowest three energy subbands in the quantum well plotted as a function of GaN electron-gas density. The heavy dotted line shows the position of the Fermi energy.

tions, the higher subbands will become occupied and their actual energies will deviate from those shown, which were calculated assuming that only the lowest subband is occupied. The energy separation between all subbands except for the first and second is very small, so that once the electron gas concentration exceeds about 5×10^{12} cm^{-2}, many subbands become occupied very quickly, resulting in a loss of true two-dimensional behavior of the gas and a lowering of the mobility due to intersubband scattering. For this reason, in the mobility calculations which follow, we treat only the case in which the lowest subband is the sole occupied level.

III. SCATTERING MECHANISMS

Due to the multitude of previous mobility studies in various materials, the dominant scattering mechanisms are well known for all semiconductors.[20] We take into account scattering by acoustic and optical phonons, ionized impurities, and alloy disorder. In our calculations, we consider a range of electron concentrations for which degenerate-electron statistics may be used at temperatures below 60 K. In this case, the total relaxation time can be calculated as a sum of the relaxation times due to each scattering process by Matthiessen's rule

$$\frac{1}{\tau_{\rm tot}}=\sum_{l}\frac{1}{\tau_i}. \tag{7}$$

At temperatures above 80 K, the validity of this relation becomes questionable due to the relaxation-time approximation made for inelastic optical phonon scattering,[8] and because of the limited applicability of degenerate statistics. However, at these higher temperatures, the mobility in these heterostructures is dominated by scattering from polar optical phonons. Because optical phonons in GaN have such a large energy (90.5 meV) compared to the energy separation between subbands, one must take a large number of subbands into account when calculating their effects, and, in so doing, the problem changes from a two-dimensional to a three-dimensional one. This corresponds to the fact that electrons which absorb an optical phonon gain so much energy that they can be scattered completely out of the confining potential and into the bulk. Thus, in calculating the optical phonon limited mobility, we have used a variational principle method[20] and general Fermi-Dirac statistics in a three-dimensional approximation. The GaN material parameters which we used in our calculations are shown in Table I.

TABLE I. Material parameters used in our calculations.

Effective mass (m^*/m_0)	0.21
Density (g/cm^3)	6.1
ε_0	9.5
ε_∞	5.35
LO-phonon energy (meV)	90.5
Lattice parameter a_0 (Å)	4.52
Acoustic-phonon velocity (cm/s)	6.6×10^5
Piezoelectric constant (Ref. 16) (h_{14}) (V/cm)	4.28×10^7
Deformation potential (Ref. 21) (eV)	8.5
Elastic constants: c_L (dyn/cm^2)	2.66×10^{12}
c_T (dyn/cm^2)	6.2×10^{11}

A. Phonon scattering

Phonon scattering plays an important role in limiting the electron mobility in III–V semiconductors. The three most important phonon-scattering processes are deformation potential acoustic, piezoelectric acoustic, and polar optical. All three of these processes have been studied extensively in bulk semiconductors.

In MDH's, although the movement of the electrons is confined to a thin layer of perhaps 100 Å near the interface, it is usually assumed that acoustic phonons can propagate freely in all three dimensions. The relaxation time for the interaction of confined electrons with three-dimensional acoustic phonons due to screened deformation-potential scattering is given by[22]

$$\frac{1}{\tau_{\rm DP}}=\frac{3m^*a_C^2bk_BT}{16\pi\hbar^3c_L}\int_0^{\pi}S(q)^2(1-\cos\theta)d\theta, \tag{8}$$

where a_C is the deformation potential, b is the variational parameter in Eq. (6), c_L is the elastic constant, and $S(q)$, the screening factor, is

$$S(q)=\frac{q}{q+q_sH(q)}, \tag{9}$$

with

$$H(q)=\int_0^\infty dz\int_0^\infty dz'\,\chi(z)^2\chi(z')^2\,\exp(-q|z-z'|)$$
$$=\frac{b(16b^3+29b^2q+20bq^2+5q^3)}{16(b+q)^4}, \tag{10}$$

and $q_s = 2m^* e^2/\varepsilon_s \hbar^2$. The change in electron momentum q during a scattering process is related to the scattering angle θ between $\mathbf{k}$ and $\mathbf{k}+\mathbf{q}$ by $q = 2k_F \sin\theta/2$. For a degenerate electron gas, we set $k = k_F$.

For the zinc-blende structure, the relaxation time for screened piezoelectric mode scattering is calculated by[22]

$$\frac{1}{\tau_{PE}} = \frac{1}{\tau_L} + \frac{2}{\tau_T}, \tag{11}$$

where

$$\frac{1}{\tau_{L,T}} = \frac{k_B T \alpha_{L,T}}{\pi \hbar k^2} \int q S(q)^2 f_{L,T}(q) d\theta, \tag{12}$$

with

$$\alpha_L = (eh_{14})^2 \frac{m^*}{4\hbar^2 c_L} \frac{9}{32}, \qquad \alpha_T = (eh_{14})^2 \frac{m^*}{4\hbar^2 c_T} \frac{13}{64}, \tag{13}$$

and

$$f_L(q) = \frac{13 + 78(q/b) + 72(q/b)^2 + 82(q/b)^3 + 36(q/b)^4 + 6(q/b)^5}{13[1+(q/b)]^6},$$

$$f_T(q) = \frac{1 + 6(q/b) + 12(q/b)^2 + 2(q/b)^3}{[1+(q/b)]^6}. \tag{14}$$

The combination of these two scattering processes (deformation potential and piezoelectric) gives the contribution to the relaxation time from acoustic phonons. As can be seen from Eqs. (8) and (12), the acoustic-phonon-scattering rates are linear functions of temperature. This approximation is true at temperatures at which the thermal energy is greater than the acoustic-phonon energy. At lower temperatures, in the Bloch-Grüneisen regime, since only phonons with small wave vectors will participate in scattering, the relaxation times will increase superlinearly and the above expressions will overestimate acoustic-phonon contributions to the total scattering rate.[23] However, since temperature-independent processes, such as Coulomb scattering, tend to dominate the low-temperature mobility, the deviations of the acoustic-phonon-scattering rate from linearity will have little effect on the total mobility.

As stated above, since the optical-phonon energy is large (90.5 meV) compared to the energy separation of the subbands, the highly inelastic nature of polar optical scattering makes the total scattering rate the sum of many intersubband and intrasubband scattering processes. This results in a smearing out of the characteristic features of a 2DEG, the most important one being the density of electrons within the potential well. For this reason, the relaxation time for scattering of electrons in this 2DEG by optical phonons is approximated by that calculated for the bulk (three-dimensional) semiconductor case using the variational method.[20]

B. Coulomb scattering

The greatly enhanced low-temperature mobilities found in modulation-doped heterostructures over bulk semiconductors are due to the difference in the scattering of electrons from ionized impurities. In bulk semiconductors, the ionized impurities occupy the same region of space as the conduction electrons, making Coulomb scattering a very efficient process. Of course, the electrostatic interaction between an ionized donor and a conduction electron is somewhat screened by other conduction electrons. However, in order to achieve the high electron concentrations needed for efficient screening, the crystal must itself be highly doped, leading to higher concentrations of ionized impurity centers and effectively negating any beneficial screening effects.

In an $Al_xGa_{1-x}N$/GaN MDH, we consider two different types of ionized impurity scattering. The first type is scattering by residual ionized impurities in the GaN, which works as described above. The second type is scattering by the ionized donors in the $Al_xGa_{1-x}N$ barrier left behind by the conduction electrons. Since the electric field of the ionized centers drops off as the distance squared, this type of scattering is much less effective in limiting the electron mobility. A further type of Coulomb scattering which we have not considered is scattering by charges at the heterojunction interface.

In order to calculate the relaxation times corresponding to the two types of screening, we follow the standard method (see Hirakawa and Sakaki[9]), where

$$\frac{1}{\tau_{\mathrm{Coul}}} = \int_0^{\pi} \nu(\theta) d\theta, \tag{15}$$

with

$$\nu(\theta) = \frac{\pi\hbar(1-\cos\theta)}{2m^*} \left(\frac{q_s}{q}\right)^2 \int dz [S(q)F(q,z)]^2 N(z), \tag{16}$$

where $N(z)$ is the distribution of Coulombic scattering centers, $S(q)$ is given in Eq. (9), and

$$F(q,z) = \int dz' |\chi(z')|^2 \exp(-q|z-z'|). \tag{17}$$

The integral in Eq. (16) over z can be divided into three integrals, corresponding to scattering from remote ionized impurities in the doped $Al_xGa_{1-x}N$ ($-L \leqslant z \leqslant -d$) and in the $Al_xGa_{1-x}N$ spacer ($-d \leqslant z \leqslant 0$) and scattering from residual impurities in the GaN ($z > 0$). The contribution due to

ionized impurities in the spacer layer can be neglected for concentrations up to 10^{15} cm^{-3} for spacers of less than a few hundred Å.

Our calculation for the Coulombic scattering rates has been performed in a temperature-independent approximation, assuming that all scattering events involve electrons at the Fermi level. At temperatures above 100 K, when the Fermi energy starts to shift upward, the approximation is no longer valid, and overestimates the Coulombic scattering rate. However, at such temperatures, the mobility is dominated by phonons, so our results for the total mobilities are still valid.

C. Alloy disorder

Although the wave function that we have used for the 2DEG disappears at the interface, due to the finite potential barrier, some electron density will inevitably penetrate into the $Al_xGa_{1-x}N$ alloy. Thus we need to consider scattering of the electrons due to alloy disorder. Following the procedure outlined in Ref. 8, we take the relaxation time for alloy disorder scattering to be

$$\frac{1}{\tau_{\text{all}}}=\frac{m^*x(1-x)\Omega\langle V\rangle^2}{\hbar^3}\int_{-\infty}^{0}|\chi'(z)|^4dz, \tag{18}$$

where $\langle V\rangle$ is the conduction-band offset between AlN and GaN, Ω is the volume of a unit cell, x is the Al fraction in the $Al_xGa_{1-x}N$ and $\chi'(z)$ is the part of the wave function which describes the penetration of the electron gas into the alloy:

$$\chi'(z)^2=\frac{4\pi e^2}{\varepsilon_S V_0}\left(\frac{1}{2}N_S+N_{\text{depl}}\right)\exp\left[\left(\frac{8m^*V_0}{\hbar^2}\right)^{1/2}z\right]. \tag{19}$$

Alloy disorder scattering rates are quite sensitive to the electron-gas density, varying as the square of N_S. This dependence corresponds to the degree to which the electronic wave function penetrates the barrier into the $Al_xGa_{1-x}N$. As alloy disorder is a short-range interaction, the screening of this potential has been neglected. In this paper, all alloy disorder scattering times and contributions to the mobility are calculated assuming an Al fraction of 15% in the $Al_xGa_{1-x}N$ layer.

D. Other scattering mechanisms

Some effects which we have not considered are interface roughness scattering, scattering due to interface charges, and the effect of the lattice mismatch between $Al_xGa_{1-x}N$ and GaN. These scattering processes can be easily incorporated into the calculations. However, as our aim was to determine inherent mobility limits in these heterostructures, and extremely flat surfaces can be obtained through MBE growth of these structures, we have ignored interface roughness scattering. The lattice mismatch between $Al_xGa_{1-x}N$ and GaN will produce a strain field at the interface, which in turn will produce an electric field. If this field is uniform in directions parallel to the interface, it will have no effect other than to alter the transfer of electrons from the $Al_xGa_{1-x}N$ to the GaN. Otherwise, if the electric field is nonuniform, it can be expected to have some effect on the mobilities. In the absence of good estimates for the strength of this field, we have also excluded this effect from our calculations.

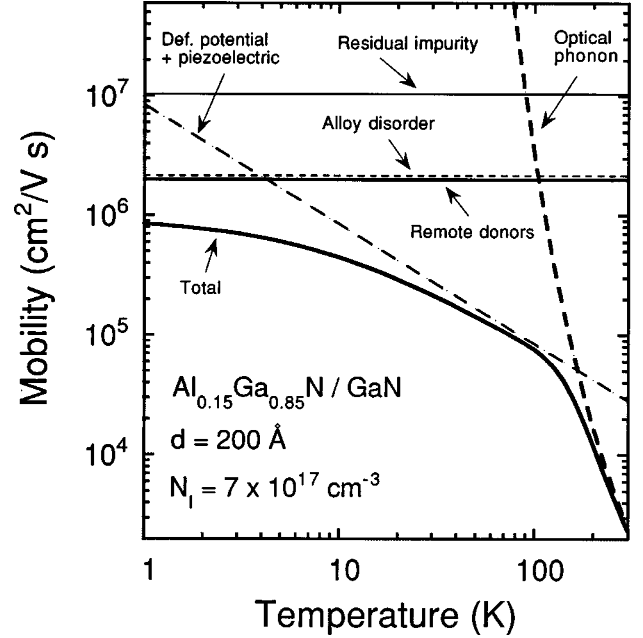

FIG. 4. Temperature dependence of the mobility in a $Al_{0.15}Ga_{0.85}N$/GaN MDH. All curves are calculated mobilities. The 2DEG density for this case is 6.2×10^{11} cm^{-2} and the concentration of residual ionized impurities in the GaN is 1×10^{14} cm^{-3}.

IV. ELECTRON MOBILITIES IN $Al_xGa_{1-x}N$/GaN MDH's

In order to see the relative importance of the various scattering mechanisms described above in determining the total mobility, we first examine the temperature dependence of the 2DEG mobility. In Fig. 4, the total mobility as well as the component mobilities of the electrons in an $Al_{0.15}Ga_{0.85}N$/GaN structure are shown as a function of temperature in the range from 1 to 300 K for a fairly ''typical'' heterostructure with a 200-Å spacer. As mentioned before, all Coulomb-type contributions were calculated in a temperature-independent approximation, so the contribution to the mobility from all types of ionic impurities appear as straight lines. Since the relaxation time for Coulombic scattering processes is inversely proportional to the impurity concentration, it is easy to recalculate this graph for different impurity concentrations.

At very low temperatures, the electron mobility is dominated mainly by alloy disorder scattering and interactions with the Coulomb field of the remote donors. Starting at about 5 K, acoustic-phonon scattering becomes the main mechanism limiting the mobility through both deformation potential and piezoelectric scattering. The strengths of both types are roughly equal. Of course, the exact temperature at which acoustic-phonon scattering becomes dominant will depend on the remote donor concentration as well as the spacer width and alloy composition of the $Al_xGa_{1-x}N$ layer. As one would expect, at temperatures above 170 K, the mobility is limited by polar-optical-phonon scattering.

As we can see from Fig. 4, the inherent mobility limit in this particular MDH, which saturates at roughly 8×10^5 cm^2/V s is set by a combination of alloy disorder,

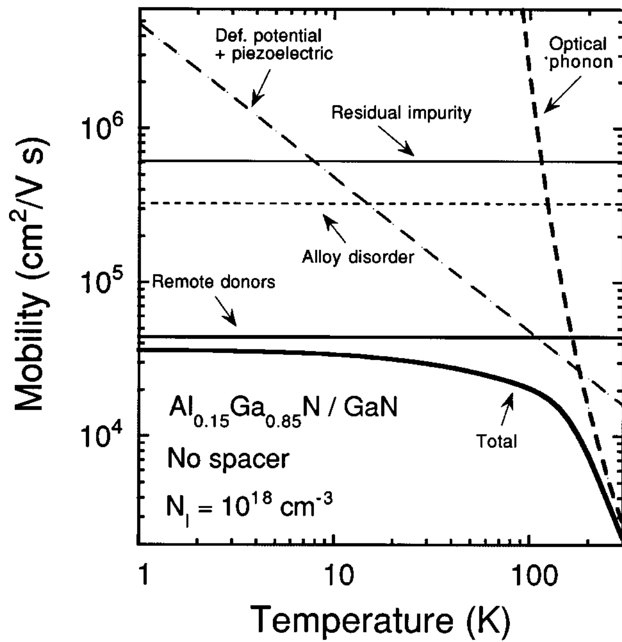

FIG. 5. Temperature dependence of the mobility in a $Al_{0.15}Ga_{0.85}N$/GaN MDH which more closely approximates what can be achieved today. The residual ionized impurity concentration in this calculation is 4×10^{15} cm^{-3} and the doping level corresponds to a electron gas density of 1.59×10^{12} cm^{-2}.

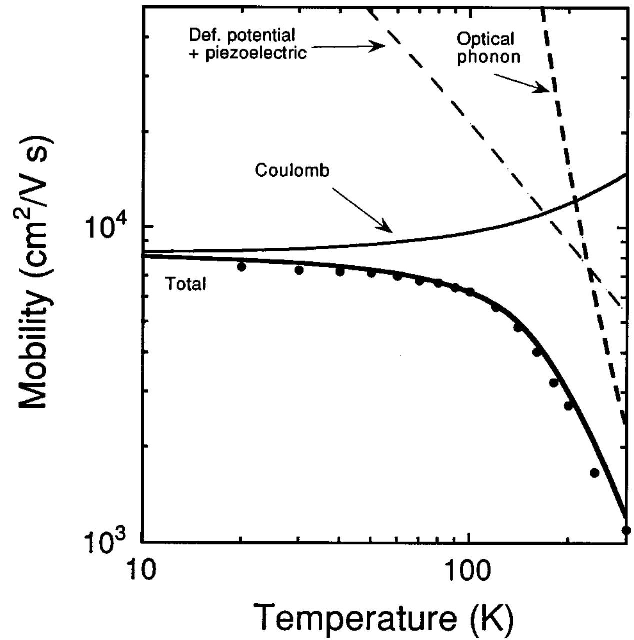

FIG. 6. Comparison of experimentally obtained mobilities (Ref. 15) with a three-dimensional model for GaN mobilities (Ref. 24). The component mobilities from optical and acoustic phonons are shown, along with a component for the contribution of Coulombic scattering from residual impurities. The theoretical curves were calculated for $N_s=6\times10^{12}$ cm^{-2}, assuming an effective width of 500 Å for the electron gas. The Coulomb scattering contribution to the mobility was adjusted in order to fit the experimental data.

remote ionized-impurity, and to a lesser extent, phonon scattering. There are several ways one could increase this inherent limit. Using wider spacers, the remote donor contribution can be made negligible even for concentrations up to 10^{20} cm^{-3}. Alloy disorder can be made less severe either by changing the Al fraction of the $Al_xGa_{1-x}N$ or by reducing the electron density which can be accomplished by growing wider spacers or reducing the remote doping concentration. By optimizing these parameters, the inherent mobility of a $Al_xGa_{1-x}N$/GaN MDH can theoretically be increased to almost 6×10^6 cm^2/V s [see Fig. 8(A)]. It should be noted however, that obtaining such mobilities puts very stringent requirements on the purity of the GaN layer. The residual charged impurity concentration must be less than 10^{13} cm^{-3}.

Figure 5 shows the calculated temperature dependence of the mobility for a MDH structure which better approximates what can be grown today. As one can see, we would expect mobilities well in excess of 10^4 cm^2/V s. However, a search of the literature shows that the highest published mobilities for such a structure are still only about 7500 with accompanying electron-gas densities of 6×10^{12} cm^{-2} or greater.[15] Comparing these densities with the results of our calculation in Sec. II, we see that, at such high concentrations, a great number of subbands must be occupied because of the extremely close spacing of the higher-lying levels. In this case, although the electrons are still confined to a channel of only about 100 Å wide, true two-dimensional behavior would not be observed in these structures due to a virtual continuum of bands being occupied, completely smearing out the effects of the z-direction quantization. The single period Shubnikov–de Haas oscillations observed with these structures is due to the spherical Fermi surface formed by the three-dimensional electron gas, the $1/H$ frequency of the oscillations corresponding to the area of the cross section of the Fermi sphere. We have modeled these experimental mobilities using a three-dimensional framework which has been described elsewhere,[24] and the results are shown in Fig. 6. We find good agreement with experimental data for a ionized impurity concentration of 1.2×10^{17} cm^{-3}. Of course at such high electron concentrations, alloy disorder scattering should also be taken into account. In order to observe true two dimension behavior, the doping level of the $Al_xGa_{1-x}N$ must be reduced so that electron-gas concentrations less than about 4×10^{12} cm^{-2} are achieved.

Another parameter which affects the mobility and may easily be varied is the electron-gas density. There are several reasons for the dependence of the electron mobility on the density. First, as the electron density increases, the Fermi energy increases, as does the magnitude of the Fermi k vector. Since most of the scattering processes that we consider are elastic, the vast majority of them occur at the Fermi energy where there are an abundant number of occupied states to scatter and unoccupied states to scatter into, and the processes themselves are dependent on the Fermi k vector. Second, as the electron density increases, the distribution of the electrons in the well changes, becoming more confined. This appears as an increase in the parameter b in Eq. (6). As can be seen from Eq. (8), acoustic deformation-potential scattering is directly dependent on b, and increases as N_s increases. Increased N_s also results in better screening of Coulomb potentials, and leads to less efficient scattering by ionized impurities. Finally, as mentioned previously, penetration of the wave function into the alloy layer increases

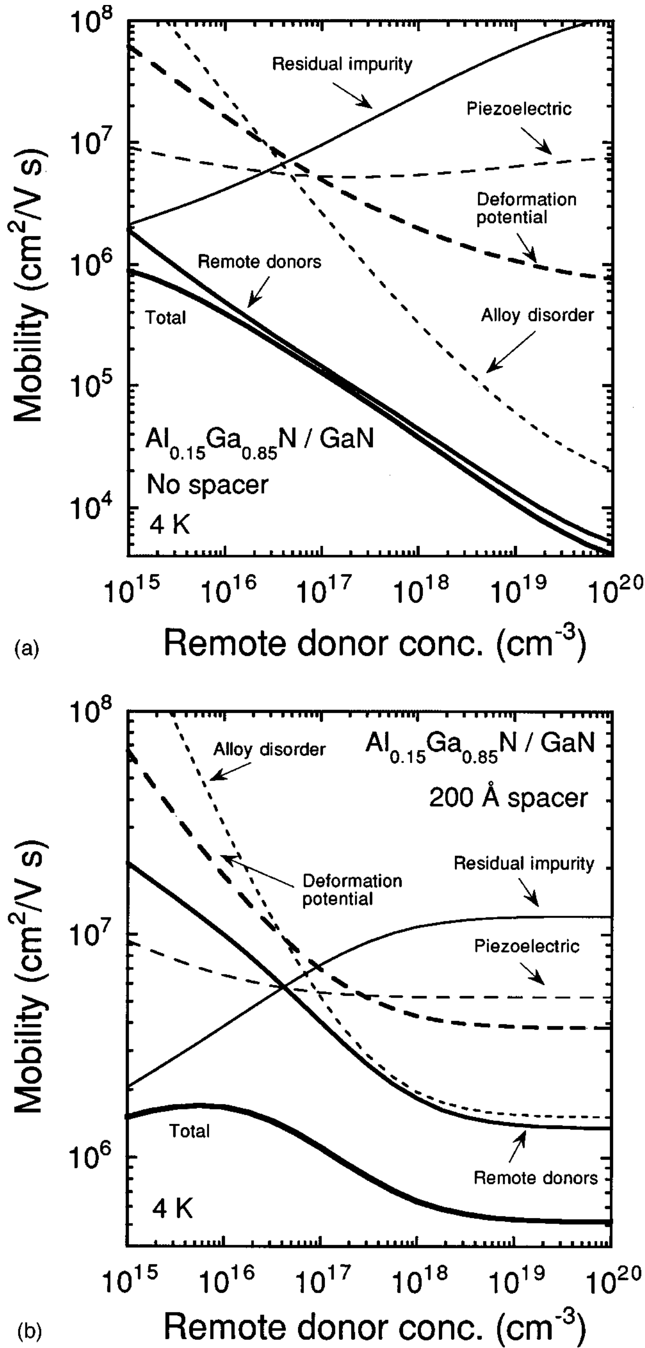

FIG. 7. Remote doping dependence of the 4-K electron mobilities in $Al_{0.15}Ga_{0.85}N$/GaN heterostructures with no spacer (A) and a 200-Å-wide spacer (B). The GaN background impurity concentration is 1×10^{14} cm^{-3} in both cases.

with the electron density, affecting the scattering rate due to alloy disorder.

The electron gas density in a MDH can be varied by several methods, such as changing the gate voltage of a high electron mobility transistor or by changing the remote doping concentration. Since the electron-gas density saturates quickly for MDH's with wide spacers, we plot the results of our calculations as a function of remote doping concentration, which is related to the 2DEG concentration as shown in Fig. 2. Figure 7 shows the remote doping dependence of the mobility at 4 K for two MDH's—one with a 200-Å spacer and one without a spacer.

For the MDH with no spacer, the dominant processes limiting the mobility is Coulomb scattering by remote impurities. At higher doping concentrations, alloy disorder also plays a significant role in reducing the mobility. In Fig. 7(B), mobilities in a MDH with a 200-Å spacer are shown. As expected, Coulomb scattering from remote donors is now much less important at low doping concentrations—residual ionized impurities in the GaN now account for the bulk of the scattering. If this background-ionized impurity concentration can be reduced further, we may reach a point where piezoelectric mode scattering by acoustic phonons is the dominant effect. As the remote doping concentration (and thus the electron-gas density) is increased, the Coulomb fields of the residual impurities are effectively screened, causing that component of the mobility to increase. Although the remote donors are more effectively screened as well, the increase in their number leads to an overall lowering of that contribution to the mobility. Scattering by alloy disorder also becomes important at high electron densities. Another feature of the results shown in Fig. 7(B) is that, above remote doping concentrations of 3×10^{18} cm^{-3}, the mobility levels off. Looking at Fig. 2, we see that, for heterostructures with a 200-Å spacer, the electron density saturates at this doping concentration due to the potential drop across the spacer, and thus there is no further appreciable change in the number of remote ionized donors or of the penetration of the electron wave function into the alloy.

Finally, we examine the dependence of the mobility on the spacer width. In Fig. 8(A), the total 4-K mobility is plotted as a function of remote doping concentration for a variety of spacer widths, assuming a residual impurity concentration of 10^{13} cm^{-3}. It should be kept in mind that for each different spacer, however, the same remote donor concentration can result in very different electron concentrations. For the smaller spacer widths, the mobility decreases as the remote doping concentration is increased due to Coulombic scattering from the remote donors as shown in Fig. 7. For larger spacer widths, the electron mobility is governed almost exclusively by piezoelectric mode acoustic-phonon scattering and Coulomb scattering from residual charged impurities in the GaN. The remote donors are too far away to be effective and the electron-gas density is too low for alloy disorder scattering to play any significant role. However, due to the large spacer width, the electron density is low enough so that the residual charged impurities are not well screened. If the residual ionized impurity concentration is higher, such as 10^{15} cm^{-3}, it is no longer advantageous to have such a large spacer. In that case, as can be seen from Fig. 8(B), the highest mobilites are actually attained by growing only a 200-Å spacer with a remote doping concentration of 10^{17} cm^{-3}, which from Fig. 2 corresponds to $N_s=4\times10^{11}$ cm^{-2}, as compared to the other spacer widths for which we have made calculations. For larger spacers, the electron density is simply not large enough to screen any residual charged impurities in the GaN effectively.

Another situation in which a larger N_s is desired is in device applications, in which it is often the conductivity, (the product of the electron charge, the mobility, and N_s) which is the critical parameter which must be maximized. Figure 9(A) shows the conductivity plotted for a number of different spacer widths at 4 K. In each case, the conductivity has been

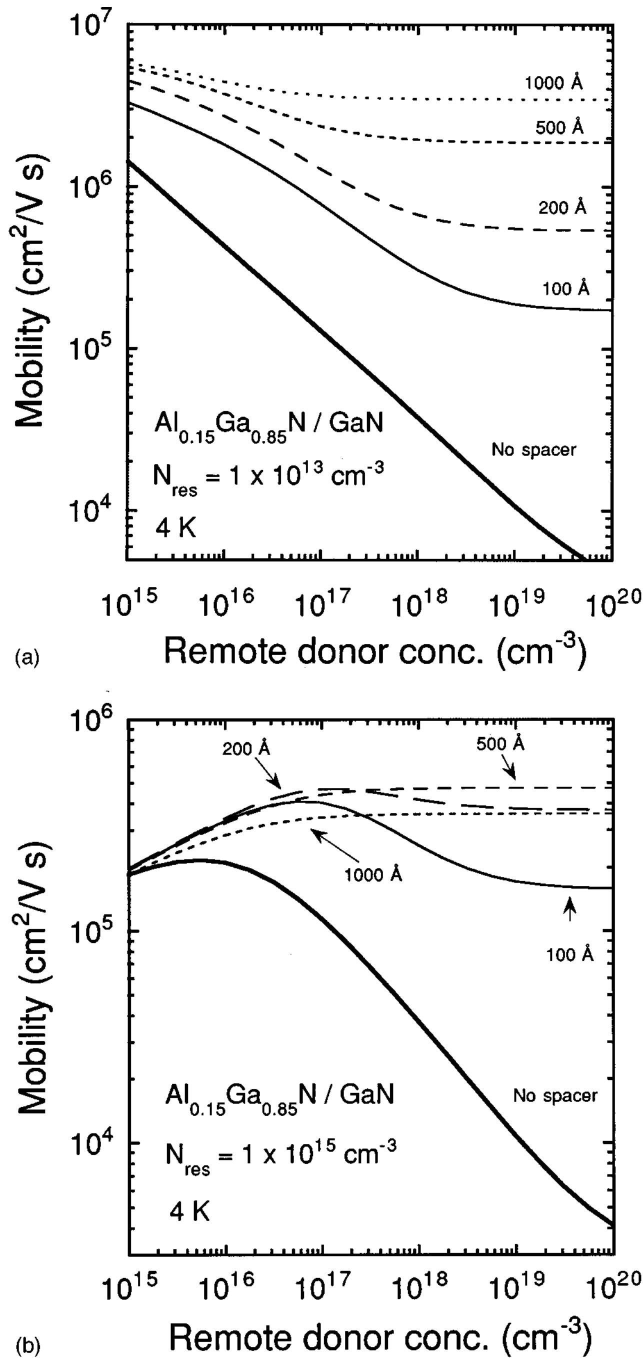

FIG. 8. Mobility plotted as a function of remote doping concentration for a variety of spacer widths. For low residual ionized impurity concentrations, a large spacer leads to the highest mobilities (A). However, if residual charged impurity are present at a high level, smaller spacers, leading to larger electron densities, are often desirable (B).

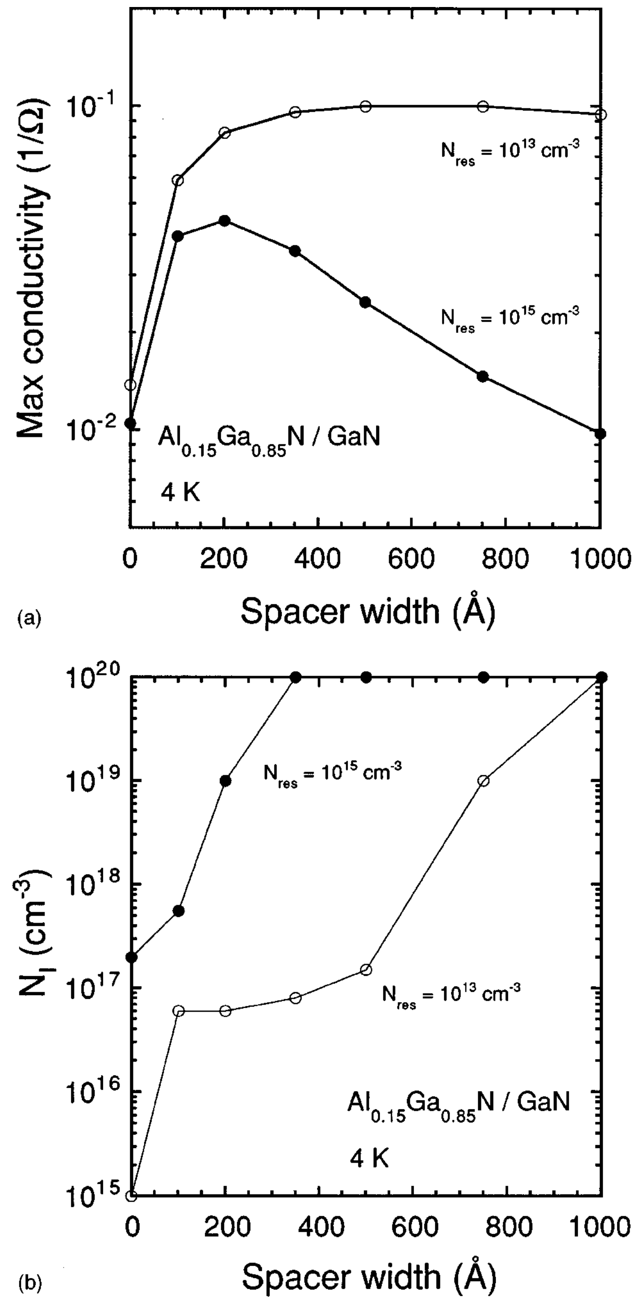

FIG. 9. (A) Maximum conductivity plotted for seven different spacer widths for $Al_{0.15}Ga_{0.85}N/GaN$ MDHs with two different residual impurity concentrations, 10^{15} and 10^{13} cm^{-3}. (B) Remote doping concentration at which maximum conductivity is achieved, plotted for the same spacer widths, again for two different values of residual impurity concentration.

maximized with respect to the remote doping concentration, for concentrations in the range between 10^{15} and 10^{20} cm^{-3}. In Figure 9(B), the doping concentration at which the maximum conductivity is achieved is plotted for the same spacer widths. Again, as with the mobility, the combination of parameters which produces the highest conductivity depends on the residual charged impurity concentration in the GaN layer. If it can be made very small (say, 10^{13} cm^{-3}), then to maximize the conductivity, a 500-Å spacer layer should be grown and the remote doping concentration should be 1.5×10^{17} cm^{-3}. On the other hand, if growing pure GaN is a problem, and residual impurities cannot be reduced below 10^{15} cm^{-3}, then the spacer should only be made about 200-Å thick and the $Al_xGa_{1-x}N$ layer should be much more heavily doped (about 1×10^{19} cm^{-3}) in order to maximize the conductivity.

V. SUMMARY

We have presented the results of electron mobility calculations for $Al_xGa_{1-x}N/GaN$ heterostructures. In our model,

we calculated the shape of the potential well and the electronic wave functions as self-consistently as possible using analytic solutions. All major scattering mechanisms were included in the mobility calculations under the conditions that only one subband be occupied. The dependence of the mobility on temperature and remote doping concentration was shown, and various strategies for achieving maximum mobilities and conductivities were described. The inherent maximum mobility attainable in such a structure is about 6×10^6 cm^2/V s for very low remote doping concentrations and large spacer widths at low temperature. Maximum conductivities are obtained at smaller spacer widths.

Due to difficulties in controlling the doping of the $Al_xGa_{1-x}N$ layer, existing $Al_xGa_{1-x}N$/GaN heterostructures show electron densities far too great to display true 2DEG behavior. However, as improvements are made in the quality of these films, the necessary low densities should be achievable in the near future. Our calculations provide upper limits on the electron mobilities that we can hope to attain in these 2DEG structures in the future.

ACKNOWLEDGMENTS

The authors would like to acknowledge Eugene E. Haller for his support and his suggestions in editing this paper. This work has been supported in part by the Director, Office of Energy Research, Office of Basic Energy Sciences, Materials Science Division of the U.S. Department of Energy under Contract No. DE-AC03-76SF00098 and in part by U.S. NSF Grant No. DMR-94 17763.

[1] L. Esaki and R. Tsu, IBM Research Laboratories, Report No. RC 2418, 1969 (unpublished).
[2] R. Dingle, H. L. Störmer, A. C. Gossard, and W. Wiegmann, Appl. Phys. Lett. **33**, 665 (1978).
[3] D. C. Tsui, A. C. Gossard, G. Kaminsky, and W. Wiegmann, Appl. Phys. Lett. **39**, 712 (1981).
[4] H. L. Störmer, A. C. Gossard, W. Wiegmann, and K. Baldwin, Appl. Phys. Lett. **39**, 912 (1981).
[5] S. Hiyamizu, J. Saito, K. Nanbu, and T. Ishikawa, Jpn. J. Appl. Phys. **22**, L609 (1983).
[6] P. J. Price, Surf. Sci. **113**, 199 (1982).
[7] T. Ando, J. Phys. Soc. Jpn. **51**, 3900 (1982).
[8] W. Walukiewicz, H. E. Ruda, J. Lagowski, and H. C. Gatos, Phys. Rev. B **30**, 4571 (1984).
[9] K. Hirakawa and H. Sakaki, Phys. Rev. B **33**, 8291 (1986).
[10] *Wide Band Gap Semiconductors*, edited by T. D. Moustakas, J. H. Pankove, and Y. Hamakawa, MRS Symposia Proceedings No. 242 (Materials Research Society, Pittsburgh, 1992).
[11] *Wide-Band-Gap Semiconductors*, Proceedings of the Seventh Trieste Semiconductor Symposium, 1992, edited by C. G. Van de Walle (North-Holland, Amsterdam, 1993); also published as Physica B **185**, 1 (1993).
[12] S. Nakamura, T. Mukai, and M. Senoh, J. Appl. Phys. **76**, 8189 (1994).
[13] M. Asif Khan, A. Bhattarai, J. N. Kuznia, and D. T. Olson, Appl. Phys. Lett. **63**, 1214 (1993).
[14] M. Asif Khan, J. N. Kuznia, D. T. Olson, W. J. Schaff, J. W. Burm, and M. S. Shur, Appl. Phys. Lett. **65**, 1121 (1994).
[15] J. M. Redwing, M. A. Tischler, J. S. Flynn, S. Elhamri, M. Ahoujja, R. S. Newrock, and W. C. Mitchel, Appl. Phys. Lett. **69**, 963 (1996).
[16] M. Shur, B. Gelmont, and M. Asif Khan, J. Electron. Mater. **25**, 777 (1996).
[17] T. Ando, A. B. Fowler, and F. Stern, Rev. Mod. Phys. **54**, 437 (1982).
[18] J. Hautman and L. M. Sander, Phys. Rev. B **32**, 980 (1982).
[19] O. Gunnarsson and B. I. Lundqvist, Phys. Rev. B **13**, 4274 (1976).
[20] W. Walukiewicz, L. Lagowski, L. Jastrzebski, M. Lichtensteiger, and H. C. Gatos, J. Appl. Phys. **50**, 899 (1979).
[21] The value of the deformation potential shown here was obtained by fitting theoretically calculated mobilities to two sets of the best experimentally obtained low-temperature mobilities in GaN (Ref. 15). The only adjustable parameter was the deformation potential. One of the fits can be seen in Fig. 6.
[22] W. Walukiewicz, in *Semiconductor Interfaces and Microstructures*, edited by Z. C. Feng (World Scientific, Singapore, 1992), p.1.
[23] H. L. Störmer, L. N. Pfeiffer, K. W. Baldwin, and K. West, Phys. Rev. B **41**, 1278 (1990).
[24] L. Hsu and W. Walukiewicz, in *III-Nitride, SiC and Diamond Materials for Electronic Devices*, edited by D. K. Gaskill, C. D. Brandt, and R. J. Nemanich, MRS Symposia Proceedings No. 423 (Materials Research Society, Pittsburgh, 1996), p. 513.